INTERNATIONAL JOURNAL FOR NUMERICAL METHODS IN FLUIDS
Int. J. Numer. Meth. Fluids **31**: 721–745 (1999)

TIME EVOLUTION OF LAMINAR FLOW OVER A THREE-DIMENSIONAL BACKWARD-FACING STEP

T.P. CHIANG AND TONY W.H. SHEU*

Department of Naval Architecture and Ocean Engineering, National Taiwan University, 73 Chou-Shan Road, Taipei, Taiwan, Republic of China

SUMMARY

A numerical investigation of laminar flow over a backward-facing step is presented within the transient context. The analysis is concerned with the step geometry and flow conditions reported by Armaly *et al.* Results show that there is generally good agreement between the three-dimensional results and the experimental data for $Re < 400$, and excellent agreement with the two-dimensional results. Insight is also provided into the rich character of the end-wall-induced three-dimensional vortices in the channel downstream of the step. To this end, the topological theory is adopted to draw the particle oil streaklines on the roof, floor, step plane and the end-wall, from which lines of separation and reattachment are theoretically determined. Together with the Lagrangian particle track plot in the flow interior, light is shed on the formation of a secondary flow pattern, and thus the development of longitudinal vortices. The present transient analysis increases the understanding of the complex interaction of the end-wall-induced vortices and the mainstream flow. This helps to reveal the mechanism responsible for the increasing penetration of the three-dimensional flow structure into a region near the mid-plane of the channel, at which the flow is essentially two-dimensional. Copyright © 1999 John Wiley & Sons, Ltd.

KEY WORDS: laminar flow; backward-facing step; time evolution

1. INTRODUCTION

As the name suggests, the flow in the separation bubble is characterized as having vortices. Near the outer boundary of the separation bubble, an adverse pressure gradient in the flow exists in the sense that there is increasing pressure in the direction of the main flow. Thus, flow separation has a considerable impact on the flow structure and has been the subject of intensive study for many years. Owing to the geometrical simplicity and the availability of experimental data [1] there is a considerable incentive to study the flow in a channel with sudden expansion.

Experimental investigations into the backward-facing step problem by Armaly *et al.* [1] and Denham and Patrick [2] have shed light on some major flow features. An attempt to increase the understanding of the process by which the flow proceeds to time-dependency has prompted researchers to resort to numerical simulation of this problem. Much previous effort has focused on two-dimensional study owing to insufficient computer power, which has made three-dimensional analysis infeasible. It is only in the last few years that significant progress

* Correspondence to: Department of Naval Architecture and Ocean Engineering, National Taiwan University, 73 Chou-Shan Road, Taipei, Taiwan, Republic of China. Tel.: +886 2 23625470, ext. 246; e-mail: sheu@indy.na.ntu.tw

CCC 0271–2091/99/200721–25$17.50

Received March 1998
Revised July 1998

has been made and analyses based on the computational fluid dynamics (CFD) technique developed to the point where three-dimensional calculations have become feasible and affordable for many research institutes [3–8]. The present study is a continuation of previous investigations by the authors into steady flows over a backward-facing step [9–11]. The attention has focused on transient issues that have been much less explored. In this study, step geometry and flow conditions reported by Armaly *et al.* [1] are considered, allowing direct comparisons with the physical experiments to be made and the CFD simulation to be benchmarked.

The remainder of this paper is organized as follows. Working equations that are subject to closure boundary and initial conditions are described. This is followed by a brief description of the discretization method employed and the solution algorithm adopted. For a faithful description of the flow feature, a theoretically rigorous approach that enables the three-dimensional flow topology to be explored is used. Based on the theory of topology, results are discussed and insight into the time evolving vortical flow is provided. Finally, concluding remarks on the implications of the computed results are made.

2. WORKING EQUATIONS AND THE DISCRETIZATION METHOD

The investigation into the unsteady nature of a flow through a three-dimensional channel expansion requires the solution of a set of non-linear coupled partial differential equations, which express mass and momentum conservation. For incompressible flow, the continuity equation must not only preserve mass conservation but also enforce a constraint on the velocity field. Thus, the pressure in the following primitive variable equations has an implicit nature:

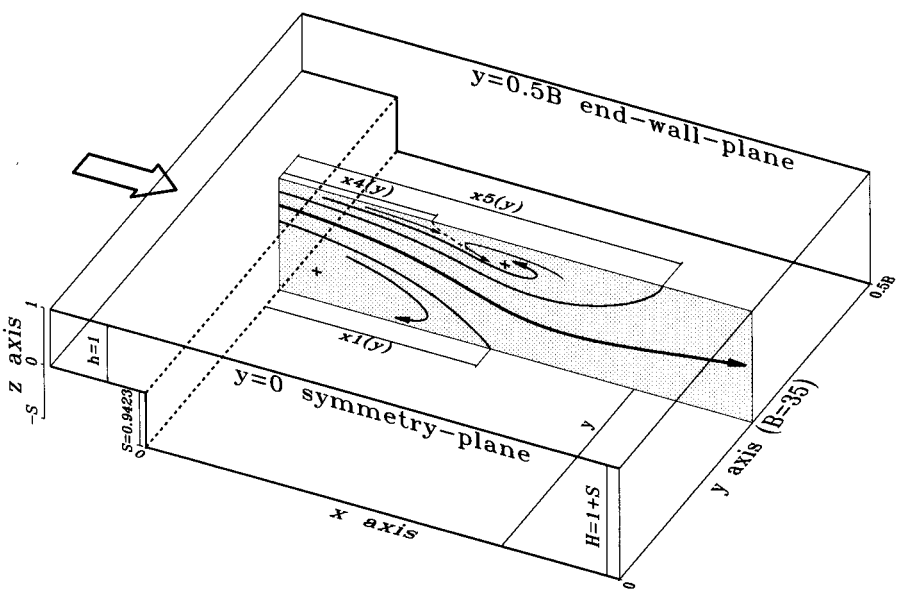

Figure 1. Geometry of the backward-facing step channel flow under investigation.

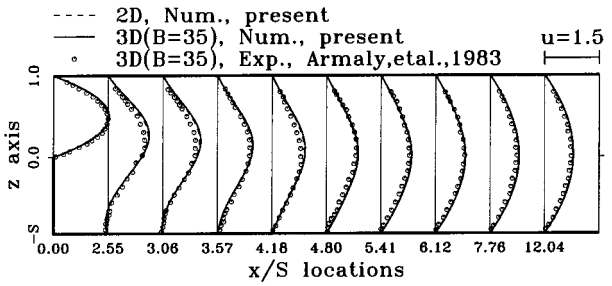

(a) Re=100

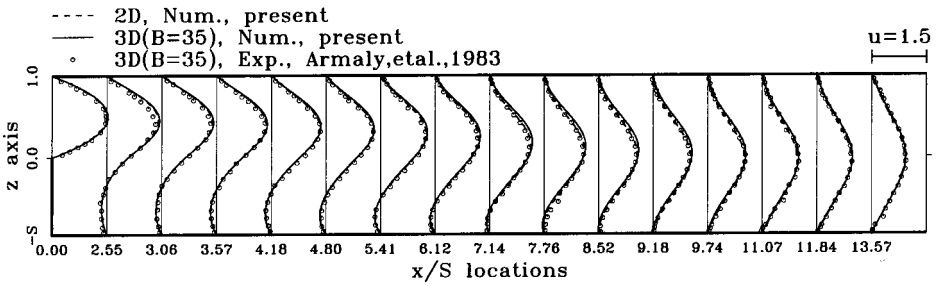

(b) Re=389

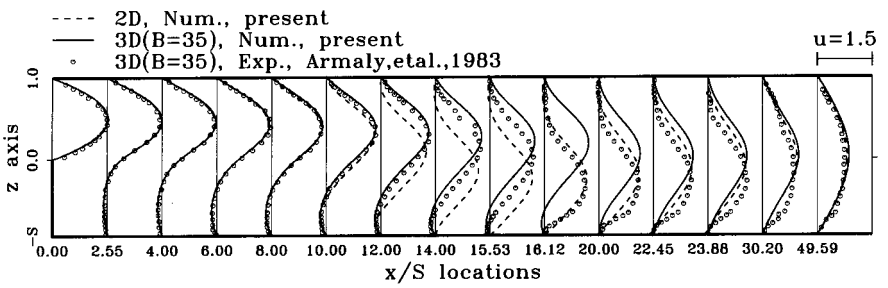

(c) Re=1000

Figure 2. Computed streamwise velocity profiles on the symmetry plane of the channel.

$$\frac{\partial u_l}{\partial t}+\frac{\partial}{\partial x_m}(u_m u_l)=-\frac{\partial P}{\partial x_l}+\frac{1}{Re^*}\frac{\partial^2 u_l}{\partial x_m\,\partial x_m}, \tag{1}$$

$$\frac{\partial u_l}{\partial x_l}=0. \tag{2}$$

In the above elliptic–parabolic mixed-type differential equations, independent as well as dependent variables are normalized to make future application an easier task. In the normalization, the mean velocity at the inlet plane U_{mean} ($\equiv 1$) and ρU_{mean}^2 are chosen as the reference quantities for the working variables $\underline{u}$ and P respectively. As for the independent variables $\underline{x}$ and t, they are made dimensionless by the upstream channel height h ($\equiv 1$) and h/U_{mean}

respectively. This leads to the Reynolds number Re^* ($\equiv \rho U_{\text{mean}} h/\mu$) shown in Equation (1). The Reynolds number definition involves the fluid viscosity, μ, and the fluid density, ρ. It is worth noting that the definition of the Reynolds number Re^* differs from Re ($\equiv \rho U_{\text{mean}}(2h)/\mu$) used by Armaly *et al.* [1]. This implies that $Re = 2Re^*$. For comparison purposes, throughout this paper, the notation of Armaly *et al.* [1] for the Reynolds number Re is adopted.

The main reason why primitive variable formulation is advocated in the flow simulation of incompressible fluid flow is that Equations (1) and (2) accommodate closure boundary conditions [12]. While primitive variable formulation is attractive for incompressible flow analysis, this formulation is not without complications. The difficulty is with a lack of working equations for the pressure. The pressure does not appear explicitly in the continuity equation (2), even though the pressure field has a direct influence on the divergence of the velocities. Thus, the pressure Poisson equation approach [13] is gaining favour as a substitute for a divergence-free equation to retain mass conservation. In addition, the usage of the pressure Poisson equation is for stability considerations since the corresponding eigensystem of the differential equations becomes well-conditioned.

The additional advantage gained in solving pressure and velocities from the coupled Navier–Stokes equations (1) and the pressure Poisson equation is that a segregated approach can be chosen. Such a solution algorithm is, in essence, an iterative approach which involves solving three momentum equations and a pressure Poisson equation by means of a cyclic predict and correct operation [13,14]. Given a pressure field, the velocities are first calculated from the momentum equations. These velocities are then adjusted to satisfy the continuity equation. The direct advantage gained from using the segregated solution procedure is that the disk space required to store the matrix equations is much reduced. Difficulties arise as to how to prescribe boundary conditions for the pressure Poisson equation. There are two ways of overcoming this problem. One can either solve the system of equations, comprising the equations of motion and the pressure Poisson equation, to avoid the specification of pressure values at the boundary nodes. Another strategy to circumvent the difficulty is to reformulate the pressure equation to its pressure correction form. In this study, discretization is conducted on staggered grids as proposed by Harlow and Welch [15]. This is useful for avoiding difficulties in the pressure boundary condition specification. Algebraic equations are obtained by integrating working equations over volume elements discretizing the three-dimensional channel. The main dependent variables are calculated on a number of staggered, interconnected grids, each of which is associated with a particular variable. A centre difference formulation is used for all the spatial derivatives except for the first spatial derivative, which governs the transport of convective fluxes. In this study, convective terms in Equation (1) are

Table I. Grid and time sizes employed in the present study

Grid	N_x	N_y	N_z	Δx (min, max)	Δy (min, max)	Δz (min, max)
Grid-C	100	85	40	(0.03, 1.0)	(0.03, 0.25)	(0.03, 0.062)
Grid-CX	150	85	40	(0.03, 0.8)	(0.03, 0.25)	(0.03, 0.062)
Grid-CY	100	120	40	(0.03, 1.0)	(0.03, 0.25)	(0.03, 0.062)
Grid-CZ	100	85	60	(0.03, 1.0)	(0.03, 0.25)	(0.016, 0.046)
Grid-D	90	25	22	(0.10, 0.55)	(0.026, 2.00)	(0.025, 0.16)

$dt = 0.02$, 0.05, 0.1, 0.2, 0.5, 1.0 and 2.0 for the transient run.
$t = [0.0, 0.1]$, [0.1, 1.0], [1.0, 2.0], [2.0, 4.0], [4.0, 10.0], [10.0, 300.0] and [300.0, 2000.0].

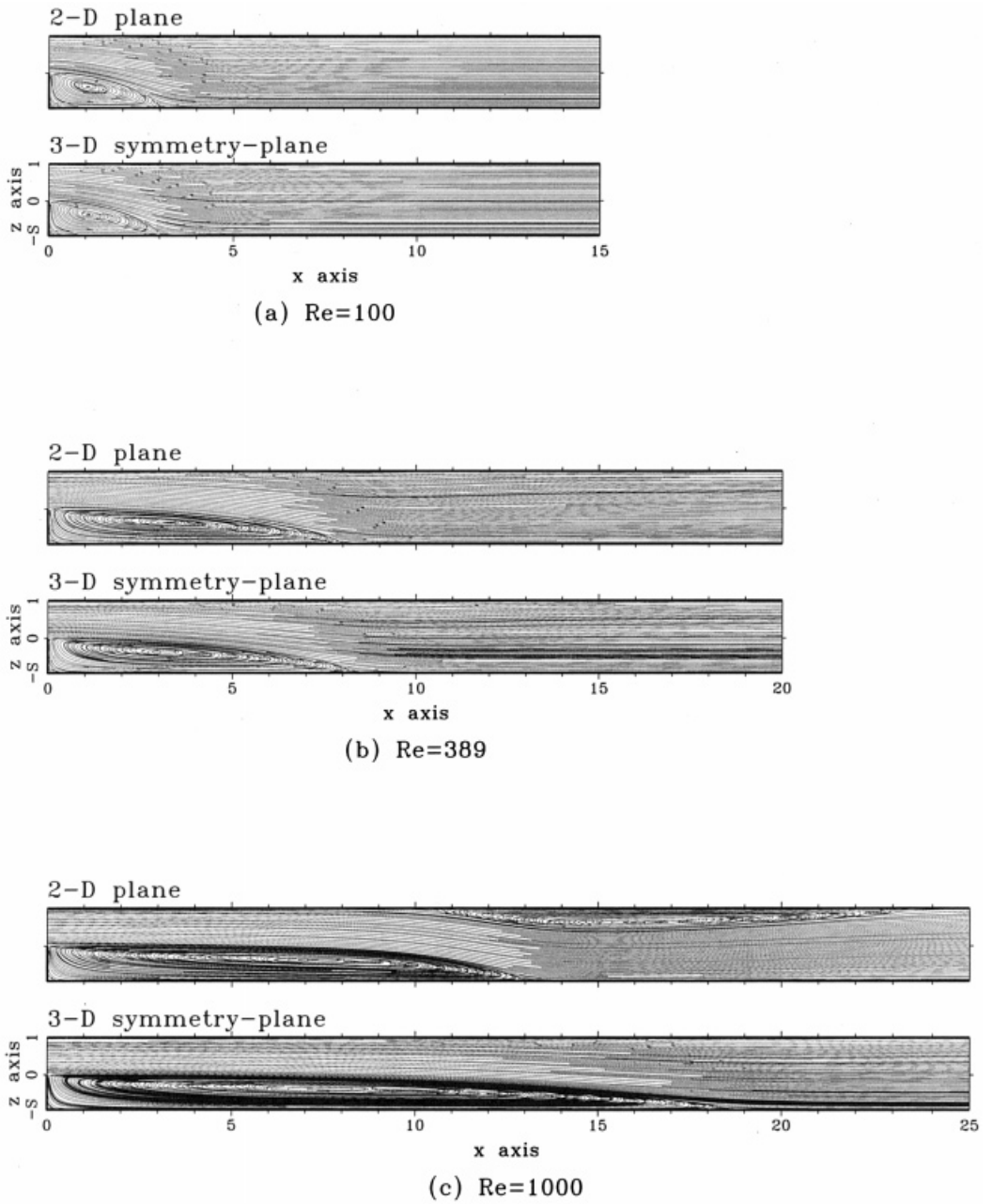

Figure 3. Computed pseudo-streamlines on the symmetry plane of the channel.

approximated using the QUICK scheme of Leonard [16]. This upwind scheme is known to produce less cross-wind diffusion error in the multi-dimensional flow analysis. In this study, the Euler implicit method is employed to approximate the time derivative term.

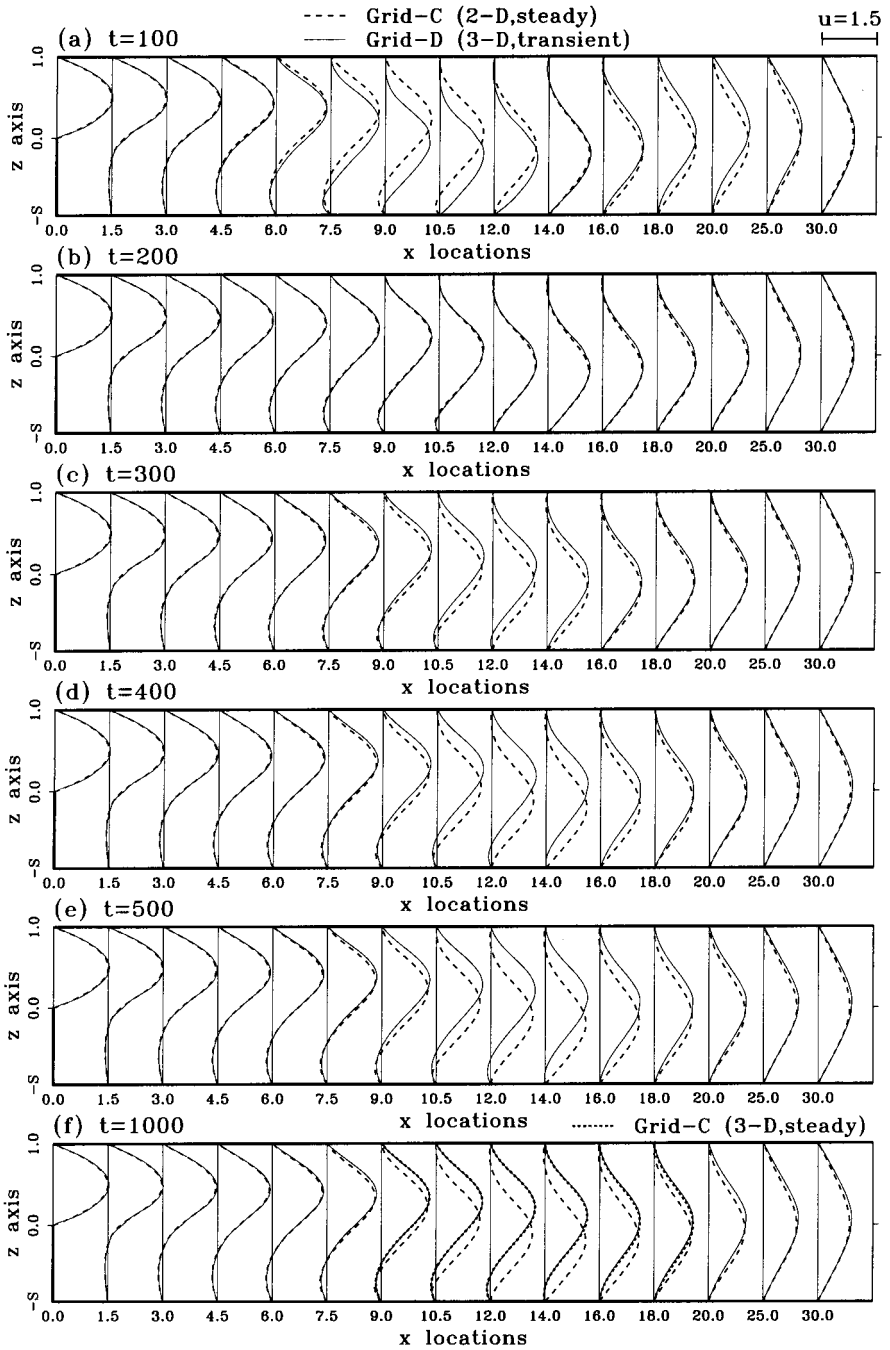

Figure 4. Time history of streamwise velocity profiles on the symmetry plane for the case of $Re = 800$.

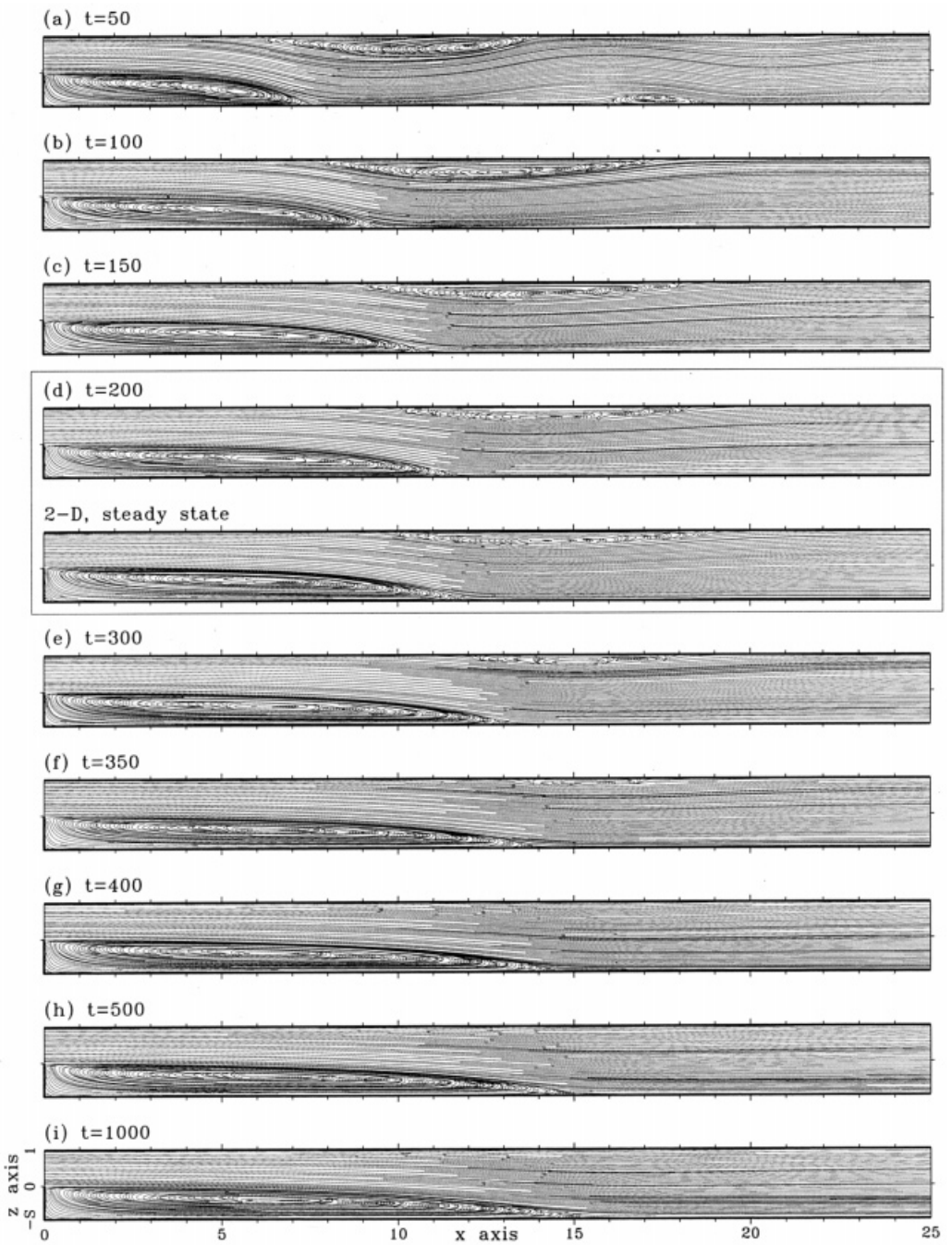

Figure 5. Time history of pseudo-streamlines on the symmetry plane for the case of $Re = 800$.

3. PROBLEM DESCRIPTION AND BOUNDARY CONDITION IMPLEMENTATION

The channel, as configured in Figure 1, is characterized as having a backward-facing step, across which a three-dimensional channel flow develops into a wider channel with an expansion ratio of $H/h = 1.9423$. Analyses were considered under conditions reported by Armaly *et al.* [1]. Direct comparisons with the physical experiments have thus been made to achieve the validation of the numerical results. Using the step geometry $S = 0.9423$ and the flow conditions of Armaly *et al.* [1], the present analysis was carried out on the basis of the Reynolds numbers $Re = 100$, 389, 800 and 1000. As noted above, these values are equal to $Re^* = 50$, 194.5, 400 and 500 respectively. Investigation into the flow conditions cited above allows the features of the flow to be investigated without the complication of turbulence. This facilitates a faithful validation of the experimental data of Armaly *et al.* [1] obtained in 1983. It is worth noting that the laminar flow assumption is experimentally supported for Reynolds numbers lower than 1200 [1].

Throughout this present analysis, inlets of the physical domain were mainly chosen at the step plane. For a faithful simulation of the experiment conducted by Armaly *et al.* [1], an upstream channel is included in the steady state backward-facing flow analysis. For this case, the inlet boundary conditions were prescribed at a plane upstream of step with a length of $10h$. Such a length is sufficient for the required parabolic entry profile to develop fully so as to permit more realistic simulation of the experimental test bed. Previous analysis revealed that inclusion of the upstream channel had a negligible effect on the flow reversal in the wider downstream channel. The difference between the reattachment length, x_1, shown schematically in Figure 1, is less than 5%. For this reason, the upstream channel was not considered here for the transient analysis to reduce the storage and computing time demands. Given the above consideration, at the step plane, a fully developed velocity profile is prescribed by

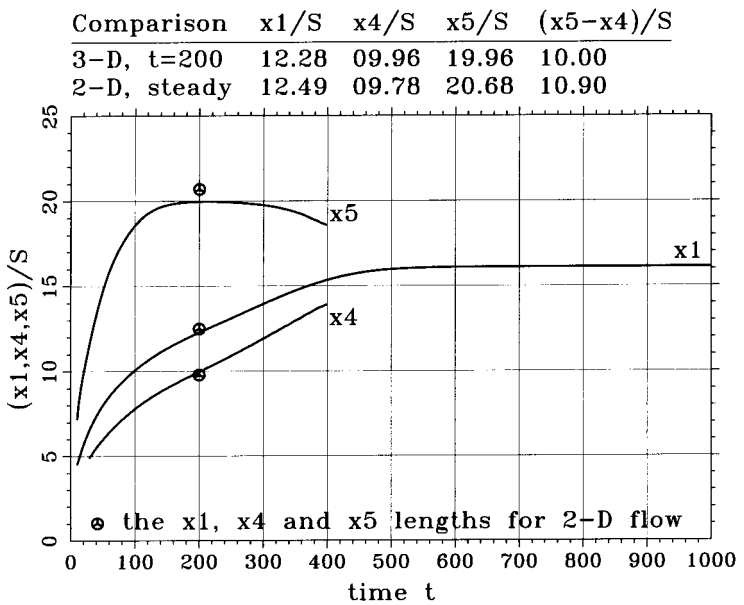

Figure 6. Time history of x_1, x_4 and x_5 lengths, computed at the symmetry plane of the channel, for the case of $Re = 800$.

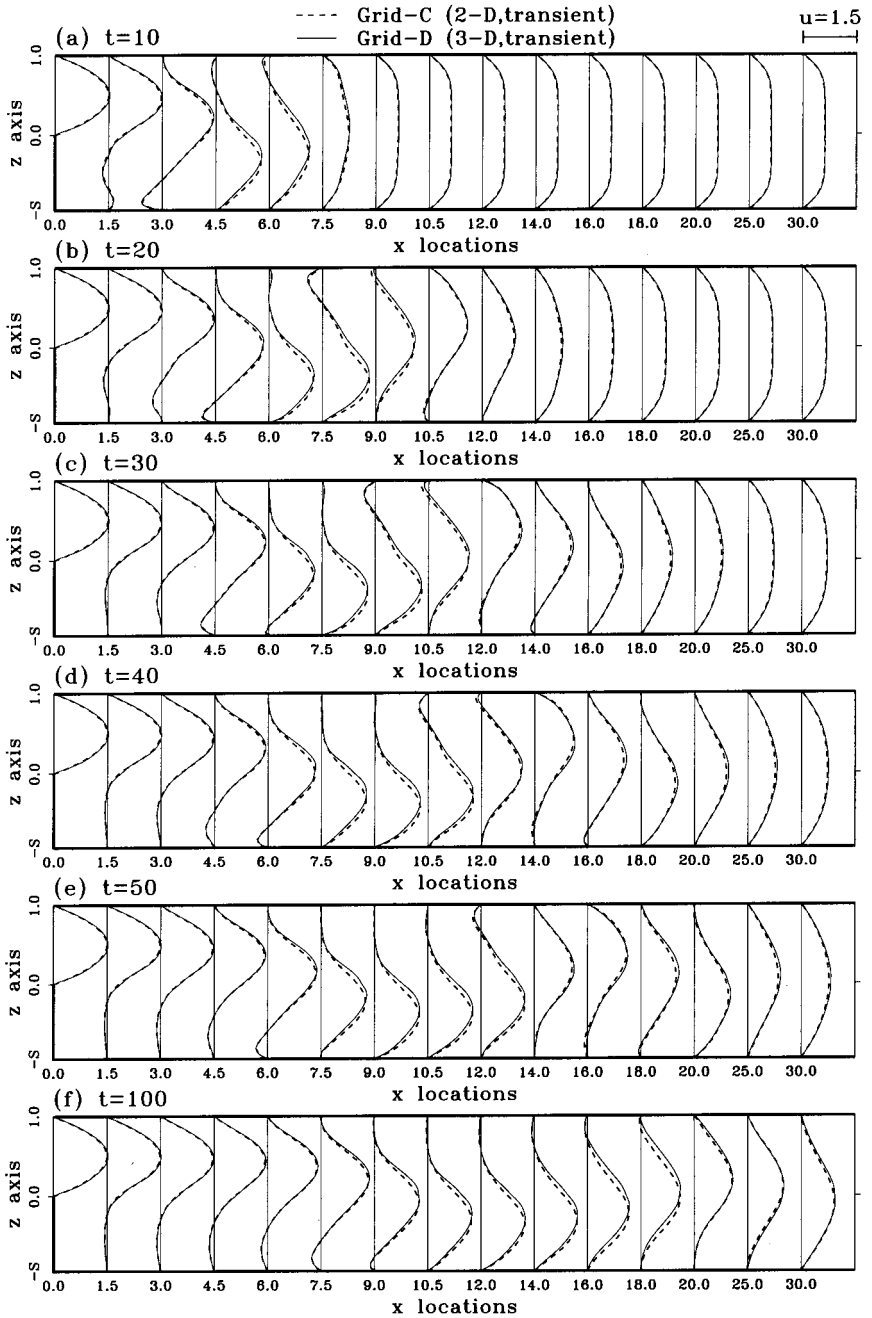

Figure 7. Time history of streamwise velocity profiles on the symmetry plane for the case of $Re = 1000$.

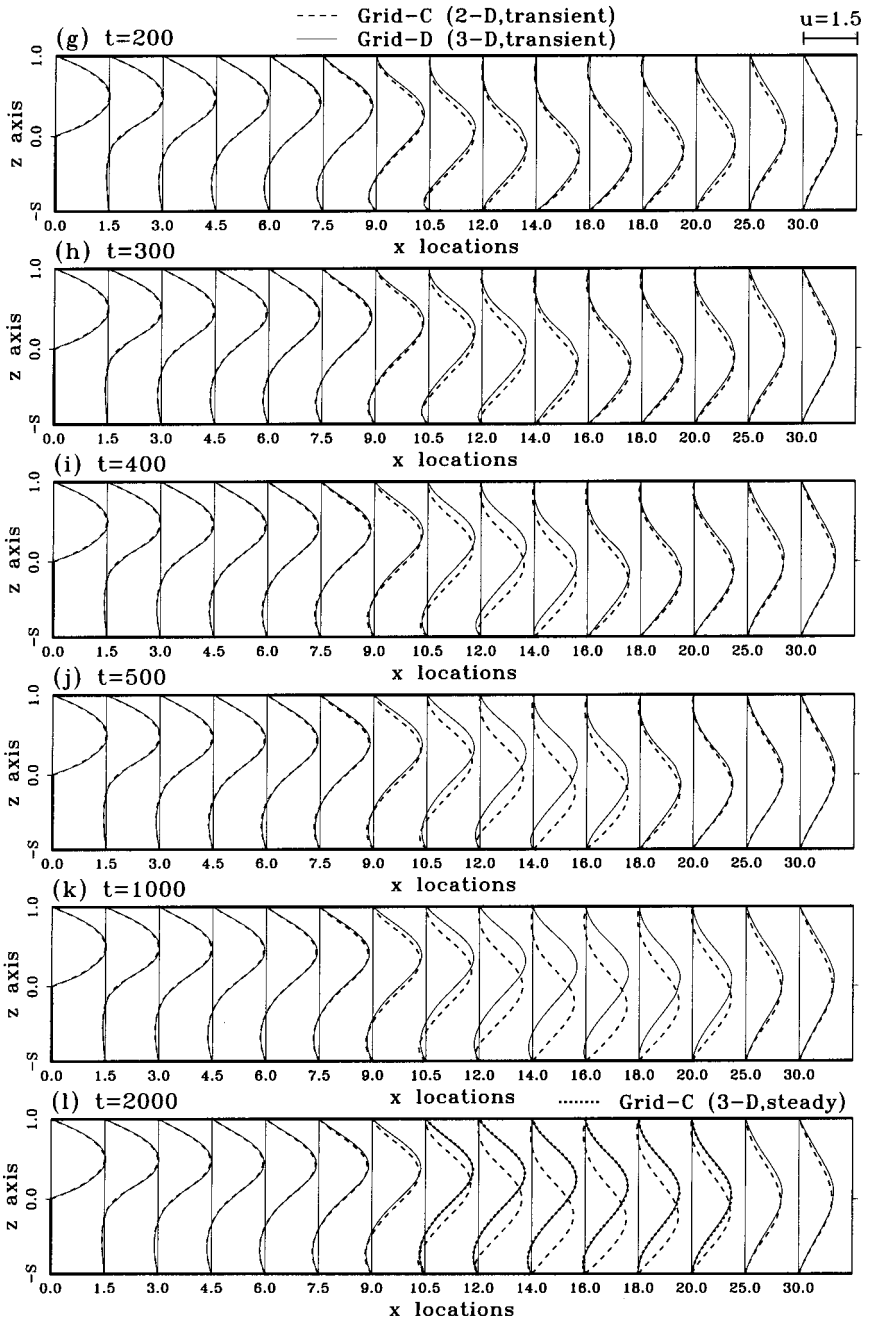

Figure 7 (*Continued*)

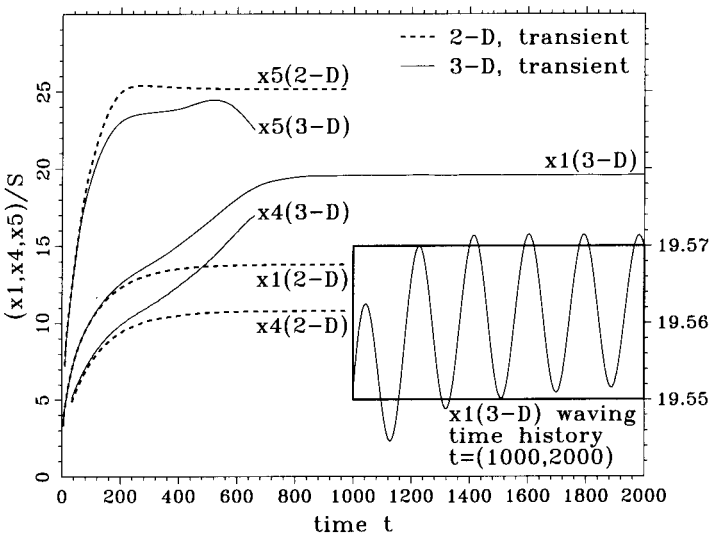

Figure 8. Time history of x_1, x_4 and x_5 lengths, computed at the symmetry plane of the channel, for the case of $Re = 1000$.

$$\underline{u} = (u, v, w) = \left(\frac{48}{\alpha\pi^3}\beta(y, z), 0, 0\right), \tag{3}$$

where

$$\alpha = 1 - \frac{192B}{\pi^5}\sum_{i=1,3,5\ldots}^{300}\frac{\tanh\xi}{i^5}, \tag{4}$$

$$\beta(y, z) = \sum_{i=1,3,5,\ldots}^{300}(-1)^{(i-1)/2}\left[1 - \frac{\cosh[(2z-1)\xi]}{\cosh\xi}\right]\frac{\cos(2y\xi)}{i^3}, \tag{5}$$

$$\xi(i) = \frac{\pi}{2B}i. \tag{6}$$

In Equations (4) and (6), B is known as the span of the channel. In the channel far enough downstream of the step plane, the flow will again be parabolic.

For practical reasons, it is desirable to truncate the analysis domain downstream of the step plane with a distance of $50h$. Truncating the analysis at the synthetic outlet is desirable; otherwise, computer time and storage requirements will greatly exceed the limits of today's computers. Thanks to the experimental confirmation of the flow symmetry about $y = 0$, it is only necessary to seek a solution in a half channel ($y \geq 0$). The problem size is thus considerably reduced provided that the symmetric boundary condition is prescribed on the mid-plane of the channel. On the rest of boundaries, where the no-slip wall assumption holds, zero velocities are prescribed on the roof, floor, step plane and the vertical end-wall.

4. RESULTS AND DISCUSSION

Before moving on to a discussion of the transient results, it is appropriate to justify the steady state calculations. Figure 2 plots the results of streamwise velocity profiles at the symmetry plane for $Re = 100$, 389 and 1000. Included in the same figure are the experimental data of

Armaly *et al*. [1] and numerical results obtained on the two-dimensional basis for comparative purposes. Grid sensitivity tests were performed by increasing grid numbers in each spatial direction. The grid details are summarized in Table I. The differences in the results obtained with three refined meshes, Grid-CX, Grid-CY and Grid-CZ, were smaller than the tolerance set in the predictions. Figures 2 and 3 show that there is generally good agreement between the present results and experimental data of Armaly *et al*. [1] and excellent agreement with

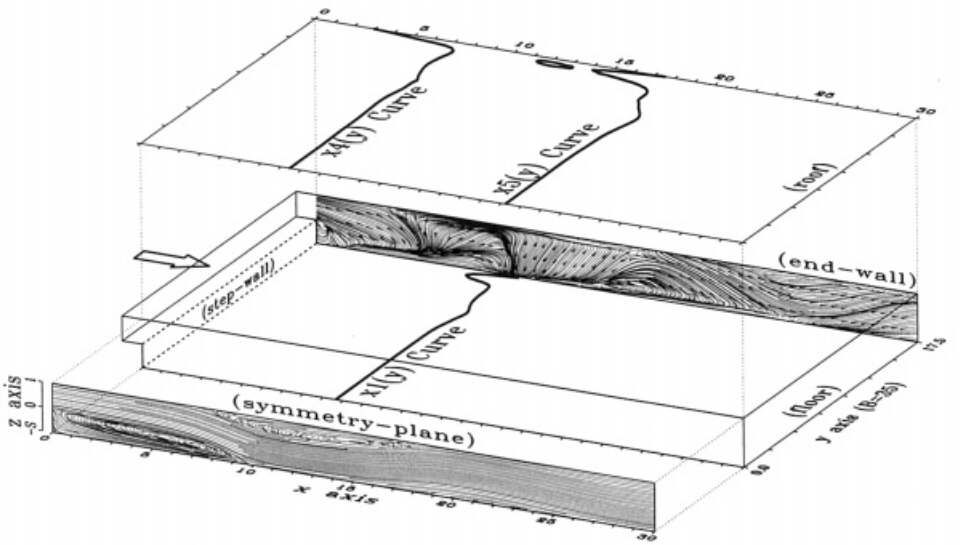

(a) t=100

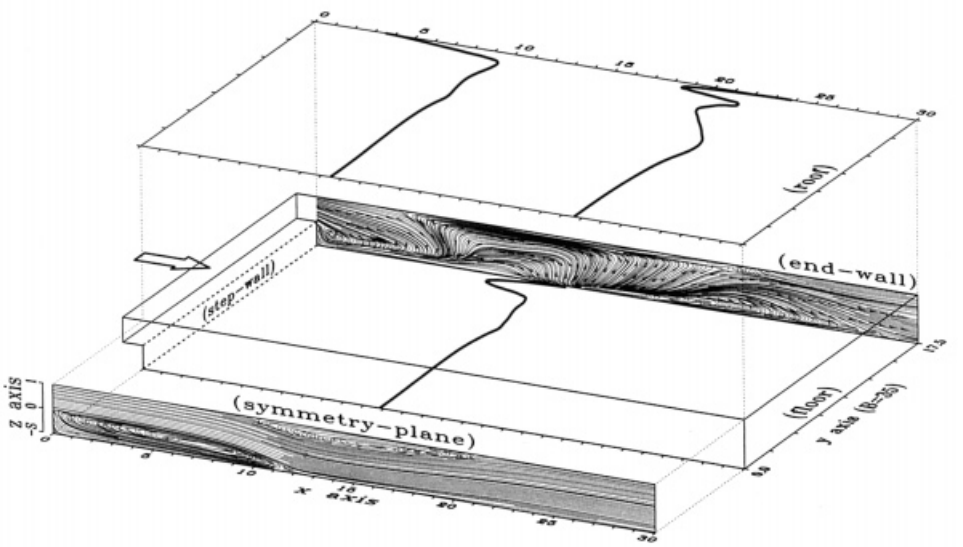

(b) t=200

Figure 9. Time history of lines of separation and reattachment plotted on the channel for the case with $Re = 1000$.

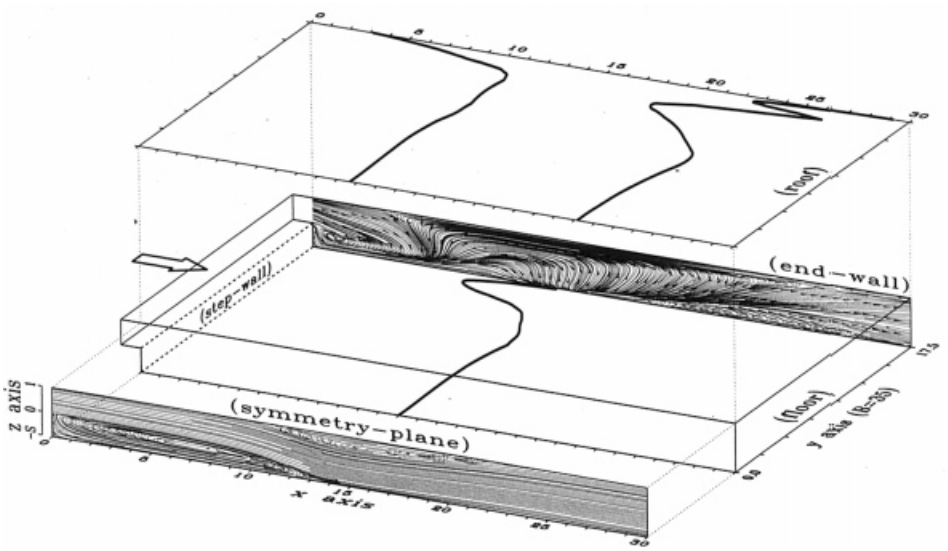

(c) t=300

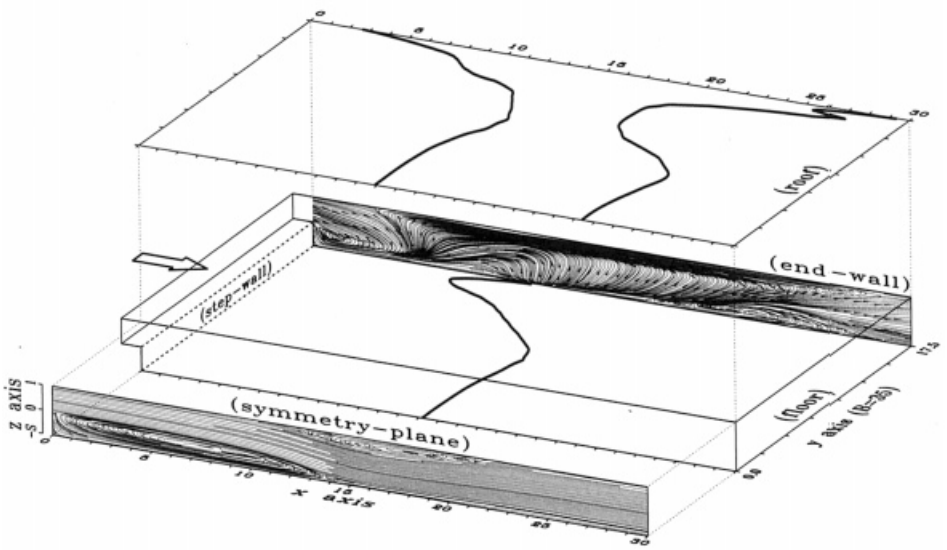

(d) t=400

Figure 9 (*Continued*)

two-dimensional numerical results for $Re = 100$ and 389. It can be inferred from these results that the channel width $B = 35h$ is sufficiently wide to ignore the end-wall boundary layer effect on the channel flow in the immediate vicinity of the mid-plane, $y = 0$, for Reynolds numbers less that 400. This is not the case as Re was increased further up to a value of approximately 1000.

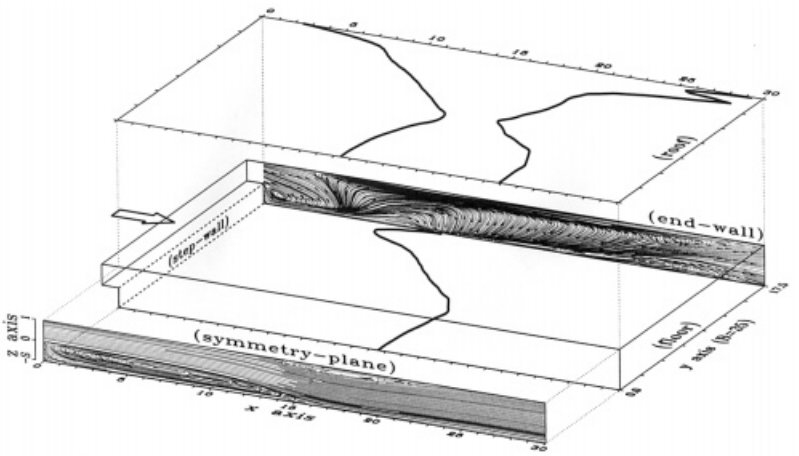

(e) t=500

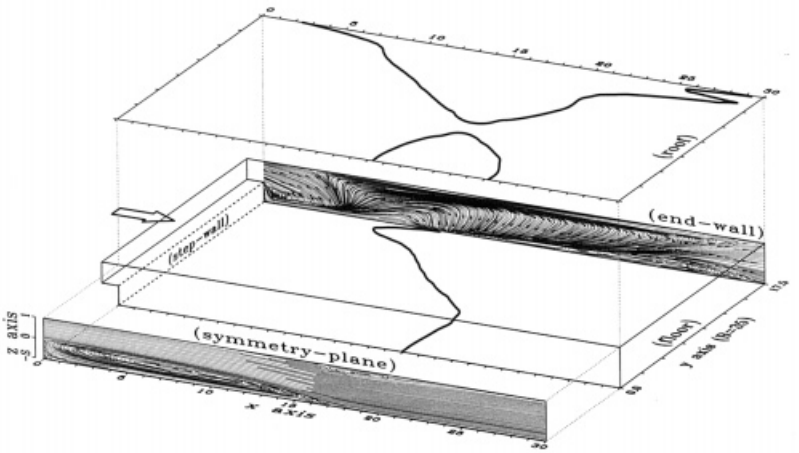

(f) t=600

Figure 9 (*Continued*)

The computed results cease to agree well with experimental or two-dimensional numerical data, as is seen in Figure 2(c), for the case of $Re = 1000$. Disagreement is particularly pronounced in the range of $10h \leq x \leq 25h$. In Figure 3(c), we find that the worst agreement is where the roof eddy (two-dimensional case) shows its presence. This raises the question of how the roof eddy can alter the flow through a channel expansion. It is the objective of this paper to determine whether the vertical end-wall will affect the flow development into the wider straight channel.

In an attempt to gain a better understanding of this phenomenon, a transient simulation of the backward-facing problem for $Re = 800$ and 1000 was conducted. In this study, Grid-C was used in the three-dimensional steady flow analysis and a coarser grid, namely Grid-D, was used in the transient analysis. For details of the grid sizes and time increments used in this study, see Table I. It is worth noting that the grid sizes of Grid-D in the vicinity of the end-wall, floor and roof of the channel are approximately the same as those discretized on the

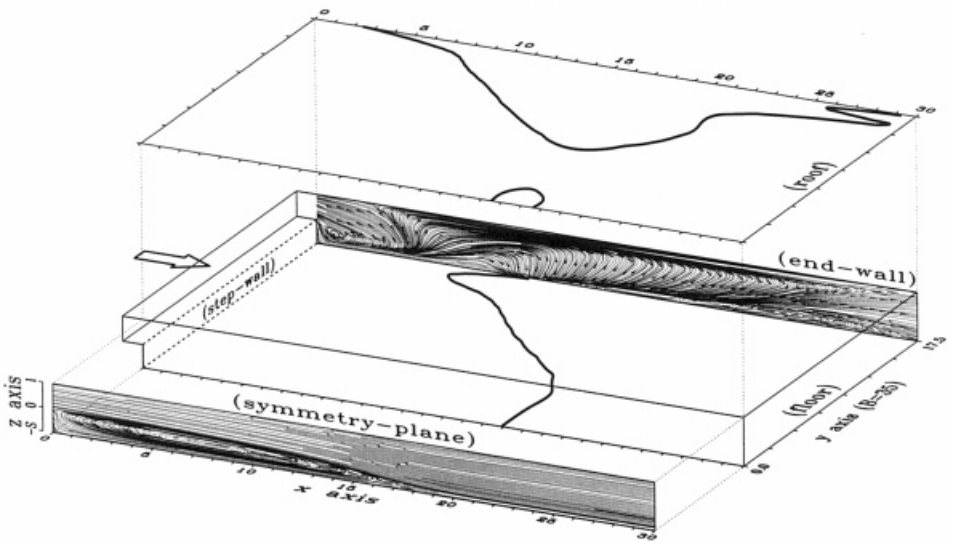

(g) t=700

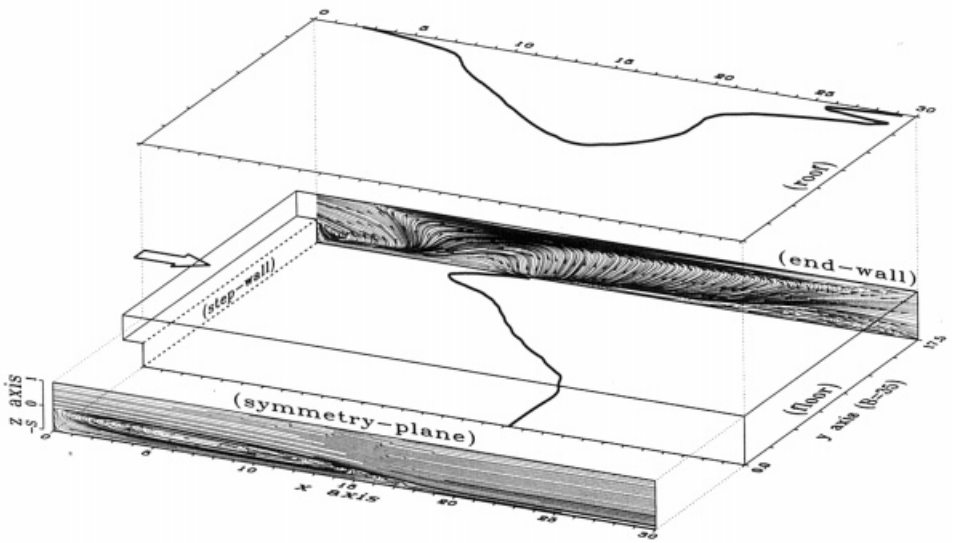

(h) t=800

Figure 9 (*Continued*)

finer grid Grid-C. As Figure 4(f), which plots the solution at $t = 1000$, and Figure 7(l), which plots the solution at $t = 2000$, show, steady state solutions are consistent with solutions computed on Grid-C. For the cases of $Re = 800$ and 1000, Figure 4 plots the time evolution of the streamwise velocity profiles at the mid-plane with time starting at $t = 100$. This is followed by the results plotted at $t = 200$, 300, 400, 500 and 1000. The corresponding streamline plots at the channel mid-plane are shown in Figure 5. In Figure 6, the time history

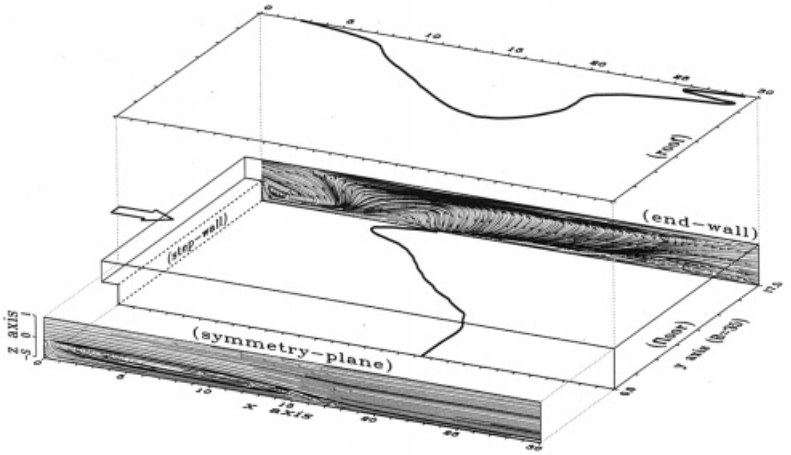

(i) t=1000

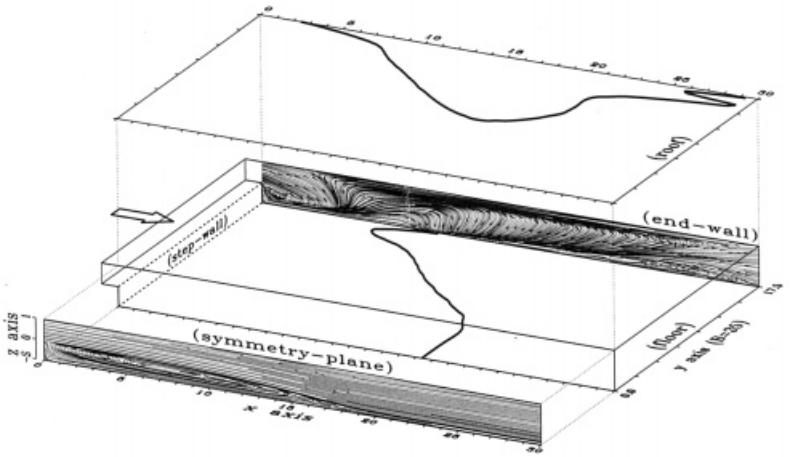

(j) t=2000

Figure 9 (*Continued*)

of x_1, x_4 and x_5 are plotted on the $y = 0$ plane. It can be seen from Figures 4(b), 5(d) and 6 that at $t = 200$, the prediction matches the two-dimensional data. Figures 5 and 6 apparently reveal that the secondary eddy on the channel roof does not exist at the mid-plane when the time reaches $t = 400$. The primary bubble separates from the step plane and reattaches to the channel floor at $x \approx 15h$. The length, x_1, remained invariant with time as $t > 500$. Careful examination of the global results, shown in Figure 6, reveals that the flow asymptotically approaches the steady state.

As the Reynolds number increases to $Re = 1000$, it can also be observed from Figures 7 and 8 the same flow nature as found in Figures 4 and 6 for the case of $Re = 800$. It can be concluded from Figures 4 and 7 that at a time $t < 100$, the flow development in the channel is primarily attributable to the step geometry. The shear stresses exerted on the end-wall are too weak to lead to a strong three-dimensional flow. In the three-dimensional transient

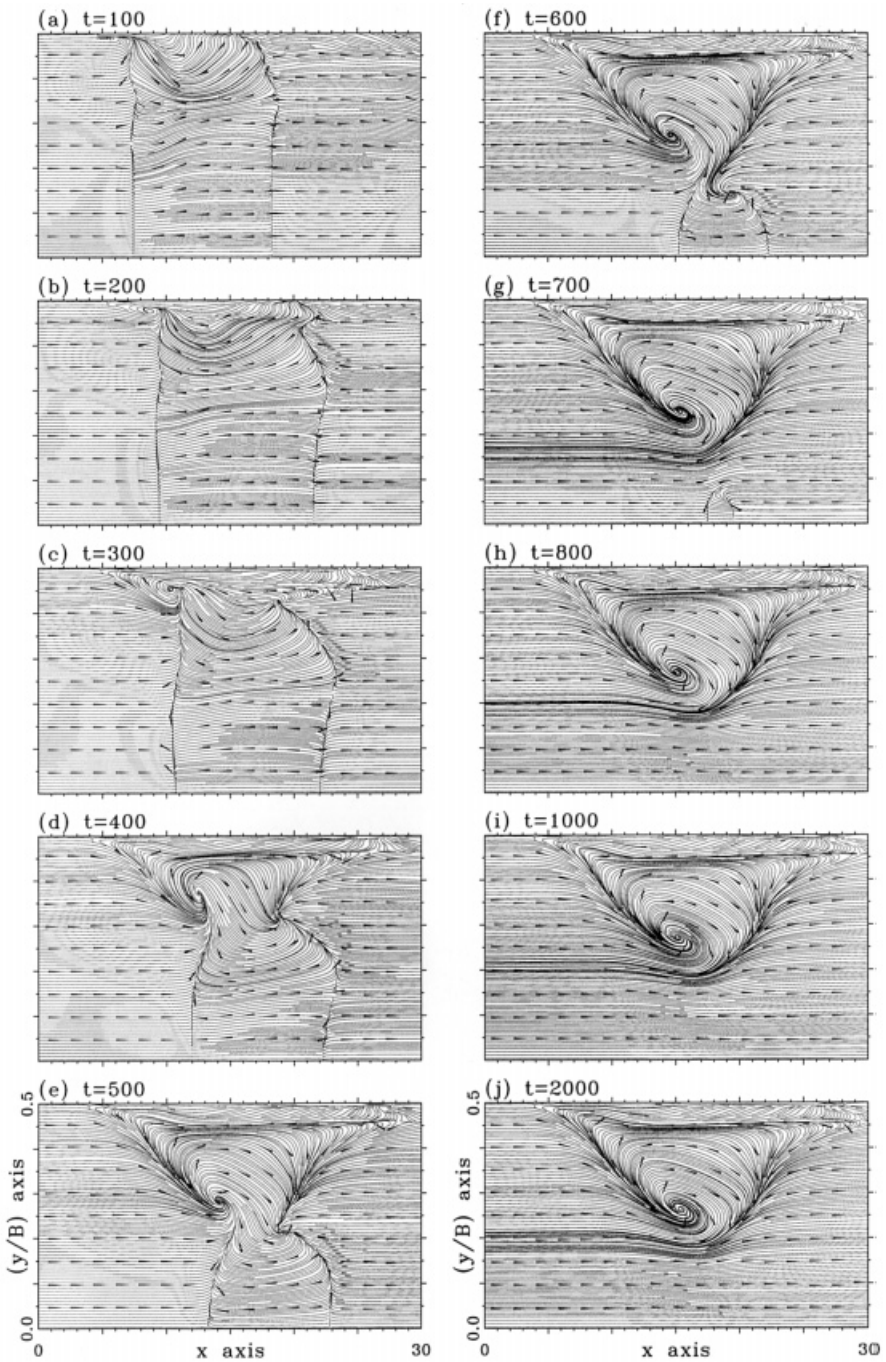

Figure 10. Time history of limiting streamlines plotted on the roof of the channel for the case with $Re = 1000$.

analysis, the streamwise velocity profiles at the plane of symmetry are not appreciably different from those of the two-dimensional results for $Re = 800$ and 1000 at a time $t < 100$. This observation is consistent with the x_1, x_4 and x_5 plots against time (Figure 8). At $t < 100$, the

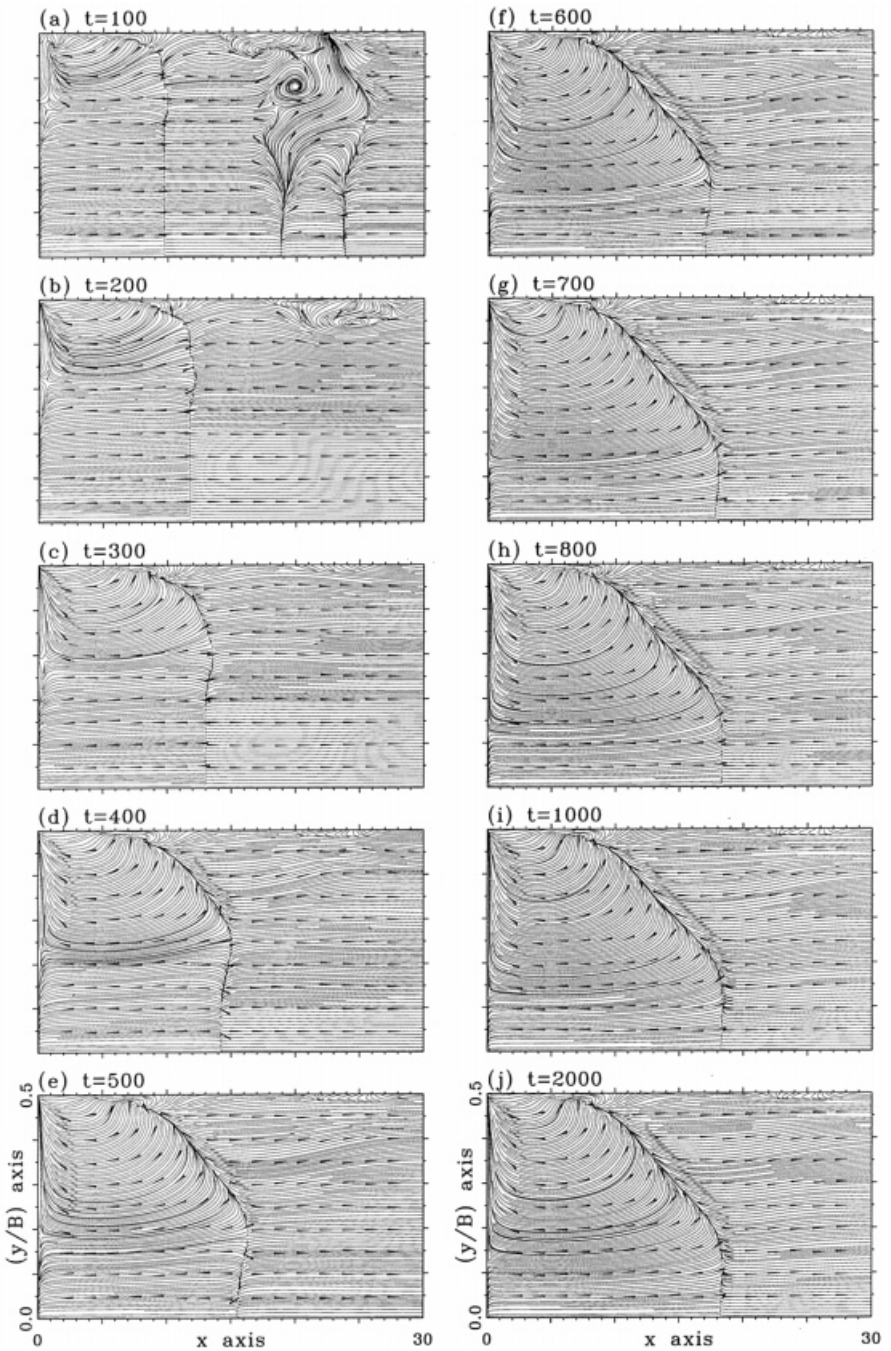

Figure 11. Time history of limiting streamlines plotted on the floor of the channel for the case with $Re = 1000$.

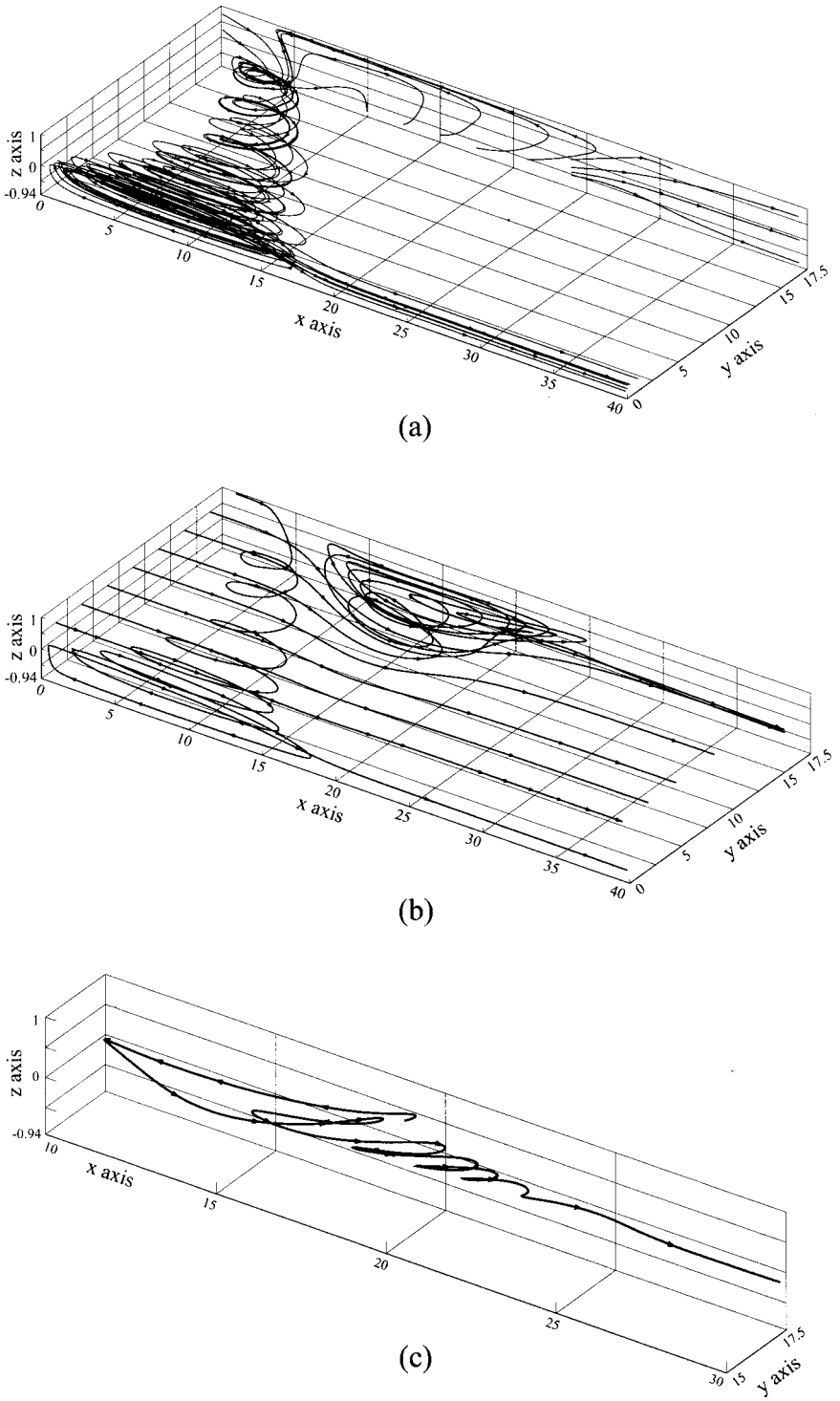

Figure 12. Lagrangian particle track for showing the spiral vortices in the channel for the case with $Re = 1000$ and with $t = 2000$: (a) end-wall particle motions; (b) step plane particle motions; (c) longitudinal vortex.

lengths of separation and reattachment do not differ between the two- and three-dimensional analyses. When the time reaches $t = 100$, the primary reattachment length starts to differ for the two analyses. The difference in the x_1 value sheds light on the influence of the end-wall on the subsequent flow development. As Figures 4 and 7 show, the three-dimensional streamwise velocity profiles on the symmetry plane no longer follow the two-dimensional profiles. This implies that at a time subsequent to $t = 100$, the end-wall effect has an increasingly important effect on the vortical flow development into the expansion channel. One can clearly see from Figure 8 a marked change in the time histories of x_1, x_4 and x_5. This explains why the two-dimensional nature of the flow evolves in the expansion flow development. Also revealed by Figure 8 is the disappearance of the roof eddy on the channel mid-plane at a time that is approximately equal to 700. Subsequent to $t = 1000$, the flow gradually reaches the periodically steady state in the sense that the oscillating amplitude of the primary reattachment length, x_1, takes on $\frac{1}{1000}$ of its mean value. The time periodicity is around 200 (Figure 8). Such a fluctuation has a tendency to decay as t keeps increasing, and finally, the flow approaches a truly steady state.

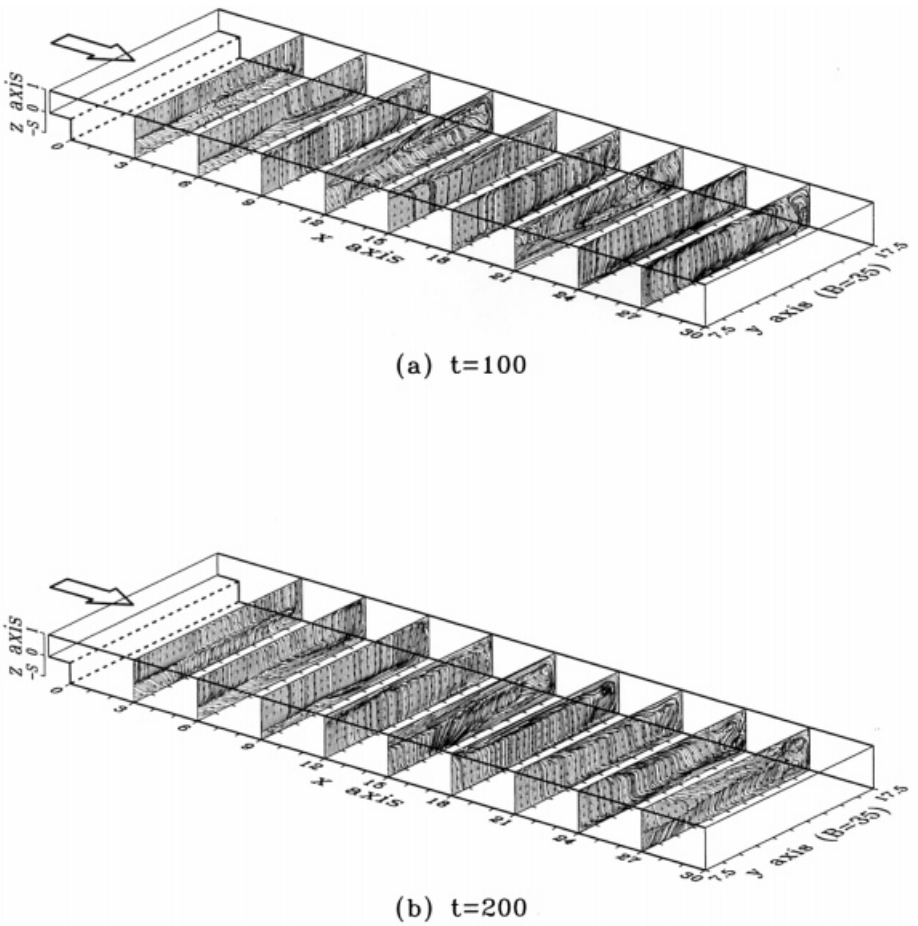

Figure 13. Time history of longitudinal secondary flow patterns plotted at selected streamwise planes for the case with $Re = 1000$.

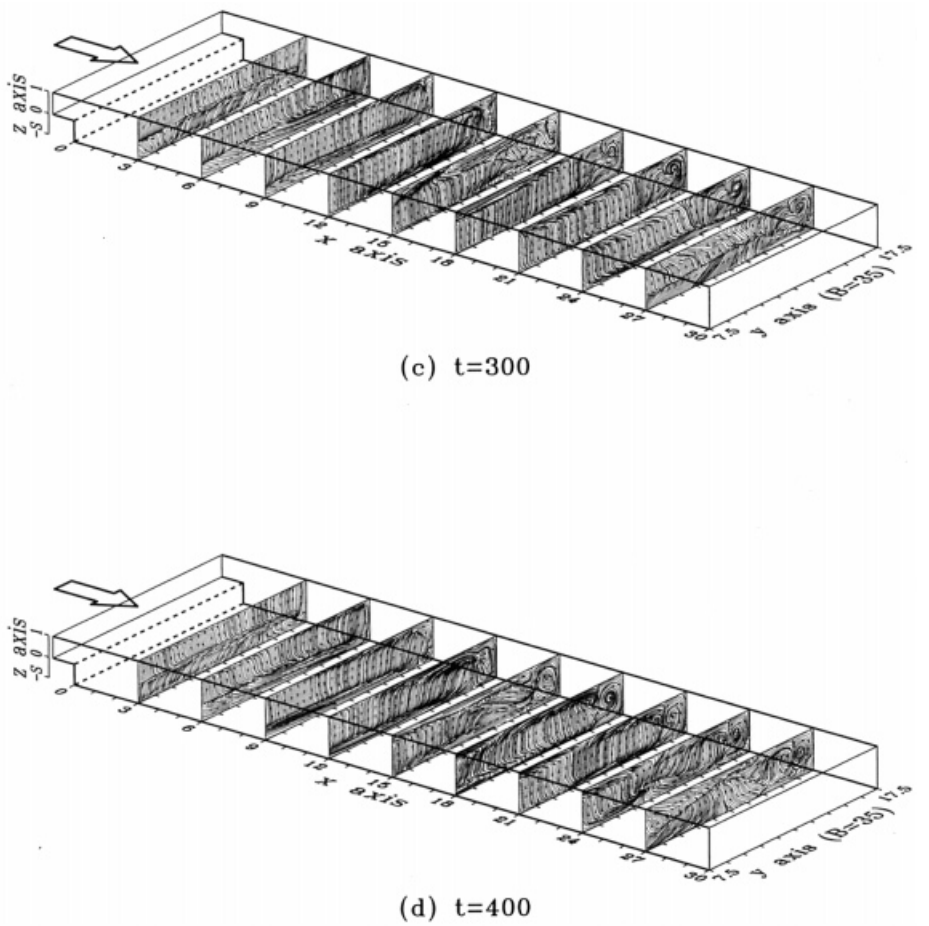

Figure 13 (*Continued*)

Given that flow separation is of fundamental importance in many processing industries, it is instructive to identify its presence. This is followed by a rigorous determination of its extension into the channel of the present interest. The present desire to depict the separation bubble prompted the adoption of the theoretically rigorous theory of topology. As suggested by Legendre [17], who advocated the use of limiting streamlines as target vectors in the topology study of vector field, limiting streamlines on the channel roof, floor and vertical end-wall are plotted in Figures 9–11. Lines of separation (x_4 curve) and reattachment (x_1 and x_5 curves) are captured and are plotted altogether in Figure 9 to provide readers with a global view of the end-wall effect on the mid-plane flow at $Re = 1000$. At the very beginning of the flow evolution, the secondary bubble does appear on the roof of the channel. This roof eddy is situated in between the lines of separation and reattachment. These initially parallel critical lines are found to extend all the way to the mid-plane (Figure 10(a)). This suggests that the end-wall effect exists only in the limited range near the end wall. As time evolves, a counterclockwise eddy is present at the intersection between the end-wall and the line of separation. This eddy is intensified through flow entrainment and convects downstream with the primary flow. The critical point, classified as a node in the nomenclature of topological

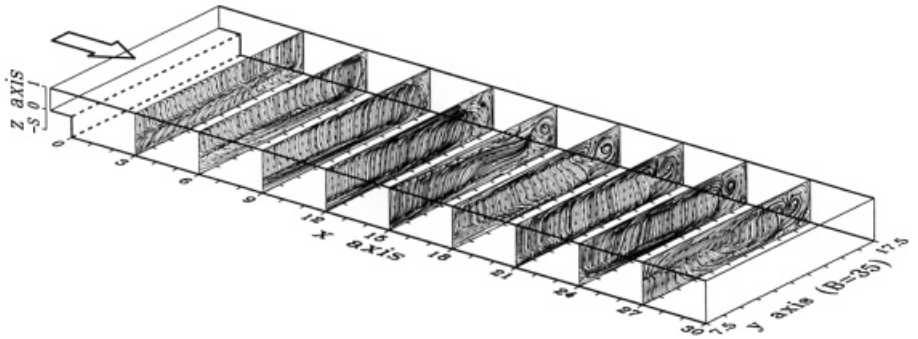

(e) t=500

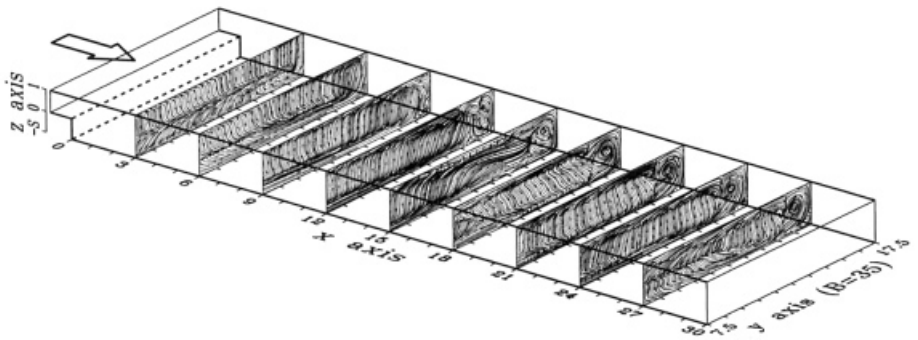

(f) t=600

Figure 13 (*Continued*)

theory, becomes clearly visible at $t = 400$. The curved separation line in turn has an effect on the adjacent pair of lines of reattachment. The line of separation curves in the downstream direction. The distortion of downstream velocity is particularly pronounced near the singular node. In contrast, the line of reattachment curves towards the upstream side. The distortion is severe in particular in the span location, where the separation line x_4 has its largest curvature near the location at $x = x_4$. As a result, the distance between the x_4 and x_5 lines reaches a minimum at the critical node. This distance continues to decrease with time; finally, at time $t > 700$, the roof eddy is only visible on the roof in the immediate vicinity of the end-wall. This plot corresponds to Figure 8, which shows that x_4 and x_5 cease to appear on the mid-plane at $t = 700$.

On the channel floor, the line of reattachment for the primary separation bubble from the computed limiting streamlines, shown in Figure 11, are clearly seen. Revealed by this figure is a slight overshoot in the re-attachment line x_1 at time $t \approx 400$. At the intersection of the step plane and the channel floor, one can observe overshoots. This critical point is by definition a separation saddle, from which streamlines repeal. This wall-oriented critical point moves towards the mid-plane as time increases. When $t > 700$, this critical point no longer varies in

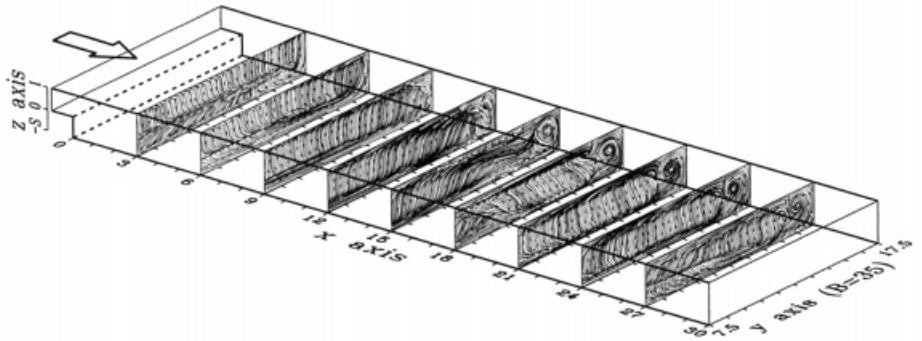

(g) t=700

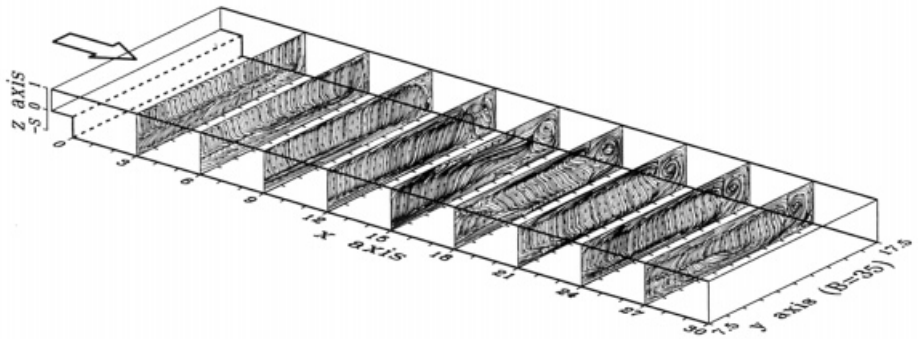

(h) t=800

Figure 13 (*Continued*)

the y-direction. For the sake of completeness, Figure 9 plots the time history of the limiting streamlines on the end-wall of the channel. Common to those oil streaklines is the spiral node present in the primary separation bubble.

At this stage, we have numerically confirmed that for Reynolds numbers smaller than 400, the flow is predominantly two-dimensional. As the Reynolds number is increased to a value above 400, the simulation results are consistent with the experimental findings in that, downstream of and in the immediate vicinity of the step, the flow is three-dimensional. It is conjectured that longitudinal vortices, which began to appear in the laminar region at $Re = 800$ [1], have destroyed the two-dimensional character of the flow. To confirm that the end-wall is the cause of the prevailing three-dimensional nature of the flow, particle tracks are plotted in Figure 12 for a particle seeded in the immediate vicinity of the end-wall (Figure 12(a)) as well as near the step plane (Figure 12(b)). The particle track reveals a three-dimensional path from the end-wall to the symmetry plane. In the approach to the symmetry plane, the particle is caught up and is entrained into the essentially two-dimensional primary eddy. The longitudinal spiralling nature of the particle track shown in Figure 12(c) is best explained by the secondary flow patterns plotted at selected streamwise locations in Figure 13.

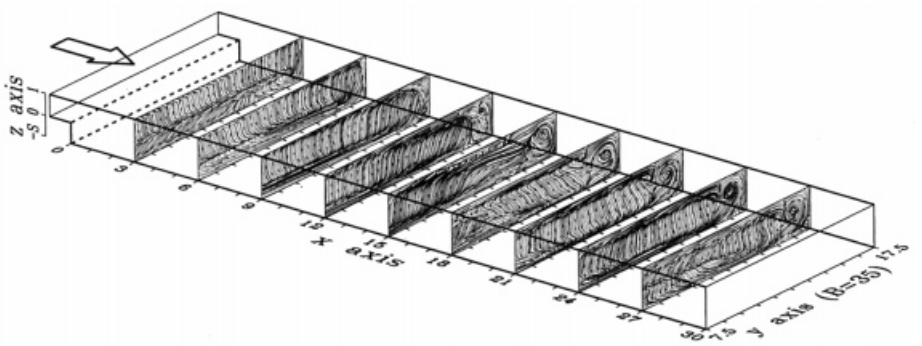

(i) t=1000

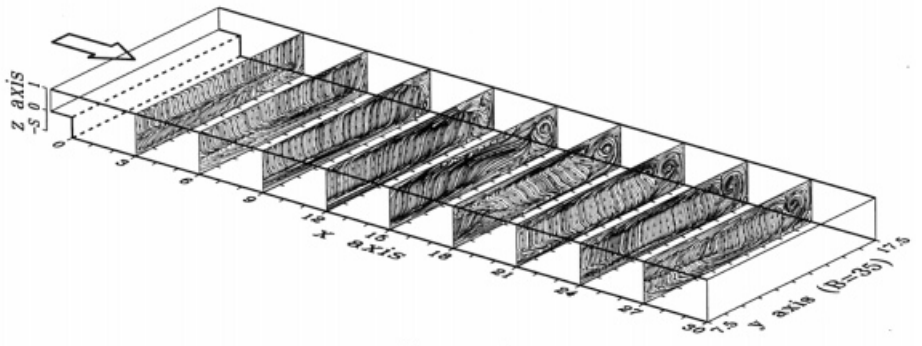

(j) t=2000

Figure 13 (*Continued*)

5. CONCLUSION

This paper has focused on a three-dimensional flow in a channel with sudden expansion since there have been relatively few computational studies. Results show that there is generally good agreement between the three-dimensional results and the experimental data for $Re < 400$. Also, the agreement of two- and three-dimensional computed results is rather promising. The results reveal that as the Reynolds number increases longitudinal vortices can evolve to the extent that the two-dimensional character of the flow is largely destroyed. Immediately away from the end wall, the x_1 curve on the mid-plane has a marked variation with the co-ordinate y. As to the secondary separation bubble on the roof of the channel, it is only visible near the end-wall. The secondary flow patterns have also been plotted to provide evidence of the complex interaction of the end-wall-induced spiralling vortices with the flow through the three-dimensional channel expansion. This transient analysis has revealed the time evolving penetration of the three-dimensional flow structure into a region of essentially two-dimensional flow near the mid-plane of the channel.

ACKNOWLEDGMENTS

The authors would like to gratefully acknowledge research support by the National Science Council under Grant NSC 87-2611-E002-027.

REFERENCES

1. B.F. Armaly, F. Durst, J.C.F. Pereira and B. Schonung, 'Experimental and theoretical investigation of backward-facing flow', *J. Fluid Mech.*, **127**, 473–496 (1983).
2. M.K. Denham and M.A. Patrick, 'Laminar flow over a downstream facing step in a two-dimensional flow channel', *Trans. Inst. Chem. Eng.*, **52**, 361 (1974).
3. D. Kwak and J.L.C. Chang, 'A three-dimensional incompressible Navier–Stokes flow solver Part 1-2NS3D code', *CFD Workshop*, University of Tennessee Space Institute, Tullahoma, TN, 1985.
4. L.J. Hou and B.N. Jiang, 'Least squares finite element solutions for three-dimensional backward-facing step flow', *Proc. 5th Int. Symp. on Computational Fluid Dynamics*, vol. 1, Sandia, JSCFD, 1993.
5. P.T. Williams and A.J. Baker, 'Incompressible computational fluid dynamics and the continuity constraint method for the three-dimensional Navier–Stokes equations', *Numer. Heat Transf. Part B*, **29**, 137–273 (1996).
6. T. Ikohagi, B.R. Shin and H. Daiguji, 'Application of an implicit time marching scheme to a three-dimensional incompressible flow problem in curvilinear co-ordinate systems', *Comput. Fluids*, **21**, 163–175 (1992).
7. P.T. Williams and A.J. Baker, 'Numerical simulations of laminar flow over a 3D backward-facing step', *Int. J. Numer. Methods Fluids*, **24**, 1159–1183 (1997).
8. B.N. Jiang, L.J. Hou and T. Lin, 'Least-squares finite element solutions for three-dimensional backward-facing step flow', *NASA-TM 106353*, 1993.
9. T.P. Chiang, T.W.H. Sheu and S.F. Tsai, 'Topology flow structure in backward-facing step channel', *Comput. Fluids*, **26**, 321–337 (1997).
10. T.P. Chiang and T.W.H. Sheu, 'Vortical flow over a 3D backward-facing step', *Numer. Heat Transf. Part A*, **31**, 167–192 (1997).
11. T.W.H. Sheu, T.P. Chiang and S.F. Tsai, 'Vortical structure in channel flows with backward-facing step', *Int. J. Turbo Jet Engines*, **13**, 277–293 (1996).
12. O. Ladyzhenskaya, *The Mathematical Theory of Viscous Incompressible Flow*, Gorden and Breach, New York, 1969.
13. P.M. Gresho and R.L. Sani, 'On pressure boundary conditions for the incompressible Navier–Stokes equations', *Finite Elem. Fluids*, **77**, 123–157 (1987).
14. S.V. Patankar, *Numerical Heat Transfer and Fluid Flow*, Hemisphere, New York, 1980.
16. B.P. Leonard, 'A stable and accurate convective modeling procedure based on quadratic upstream interpolation', *Comput. Methods Appl. Mech. Eng.*, **19**, 59–98 (1979).
17. R. Legendre, 'Separation de courant lecoulement laminaire tridimensional', *Rech. Aero*, **54**, 3–8 (1956).

